https://doi.org/10.15407/ufm.26.01.066

M.Y. HASBI[1,2,*], EFENDI[2,], and N. SOFYAN[1,3,***]**

[1] Department of Metallurgical and Materials Engineering,
Faculty of Engineering,
Universitas Indonesia, 16424 Depok, Indonesia

[2] Research Centre for Metallurgy,
National Research and Innovation Agency,
Tangerang Selatan, 15314 Banten, Indonesia

[3] Advanced Materials Research Centre,
Faculty of Engineering,
Universitas Indonesia, 16424 Depok, Indonesia

* muhyunan.hasbi@gmail.com,
** efendimabruri@gmail.com, *** nofrijon.sofyan@ui.ac.id

SYSTEMATIC REVIEW OF SUPERELASTIC FeNiCoAlTaB ALLOYS

Iron-based shape-memory alloys (Fe-SMAs) have attracted significant attention due to their unique properties and potential applications. Among these alloys, the polycrystalline Fe–Ni–Co–Al–Ta–B (NCATB) alloy stands out as a promising alternative to NiTi-based SMAs owing to its superior superelastic (SE) behaviour. The SE properties of Fe-SMAs are intrinsically linked to the thermoelastic (TE) nature of their martensitic structure. This structure is achieved through a combination of appropriate fabrication processes and thermomechanical treatments (TMTs). These processes facilitate the formation of precipitates and the development of a dominant texture along specific directions and planes. Previous research has demonstrated the remarkable SE capability of the NCATB alloy, achieving a strain value of 13.5% at room temperature. This remarkable achievement was attributed to the cold-rolling fabrication process, which involved an extreme deformation of 98.6%. However, this process resulted in extremely thin sheets (of 0.2 mm thick), posing challenges for practical applications due to the limited size and form factor. To advance the development of NCATB alloys

Citation: M.Y. Hasbi, Efendi, and N. Sofyan, Systematic Review of Superelastic FeNiCoAlTaB Alloys, *Progress in Physics of Metals*, **26**, No. 1: 64–88 (2025)

© Publisher PH "Akademperiodyka" of the NAS of Ukraine, 2025. This is an open access article under the CC BY-ND license (https://creativecommons.org/licenses/by-nd/4.0)

further, a comprehensive review is essential. Such a review will provide a foundational understanding and facilitate future research efforts by summarising the existing data and methodologies. Therefore, this review paper aims to offer an in-depth discussion of the collected research data, organised according to the evolving research methodologies. By compiling and analysing these studies, the review work seeks to highlight the current progress, identify gaps, and suggest potential directions for future research on the NCATB alloy.

Keywords: alloying, Fe–Ni–Co–Al–Ta–B, shape-memory alloy, superelasticity, thermomechanical treatments.

1. Introduction

Shape-memory alloy (SMA) is an intelligent material capable of recovering plastic deformation and returning to its original shape, when heated or when the load is released [1–5]. The main characteristics of SMA are the shape-memory effect (SME) and superelasticity (SE). To date, Ni–Ti remains the most widely used alloy in various applications of SMA materials due to its diverse advantages [6, 7]. With the development of SMA material research, an alternative alloy based on Fe has been discovered. Fe-based alloys are chosen because they have several advantages, including low raw material costs, ease of machining processes, good formability, and sufficiently high strength [8–10].

Research activities related to Fe-based SMA materials are quite extensive, involving various alloy designs and thermo-mechanical treatment (TMT) schemes to achieve optimal superelastic properties [11–15]. One of the Fe alloys that is quite intriguing in the development of SMA materials is the polycrystalline Fe–Ni–Co–Al–Ta–B alloy (NCATB). The polycrystalline NCATB alloy was firstly discovered by Tanaka *et al.* [11] in 2010, demonstrating a superelasticity value reaching 13.5% at room temperature. This value far exceeds the superelasticity capability of NiTi, which is almost double, with a value of 7% [11].

Several studies have attempted to explore the properties and potential applications of NCATB alloys. For instance, Tseng *et al.* [16] conducted a comprehensive analysis of the effect of heat treatment processes on the superelastic properties of NCATB alloys through recrystallization behaviour and precipitate formation. In his research, Tseng found that a difference of 0.5 hours in solution treatment duration resulted in abnormal grain growth, increasing grain size by up to seven times (from 210 to 1570 μm), which directly correlated with the superelastic values. Zhang *et al.* [17] investigated the influence of tantalum and NiAl precipitations at grain boundaries on the superelastic properties of polycrystalline NCATB alloys. Zhang stated that the growth of β-precipitates at the grain boundaries is preceded by the growth of Ta precipitates. Both of these precipitates degrade superelastic performance. One solution to control the growth of these precipitates is to increase the low-angle grain boundaries through

the deformation process. Zhao *et al.* [18] performed an in-depth analysis on the effect of solution treatment processes on the microstructure, macrotexture, and superelasticity of NCATB alloys. The optimal solution treatment temperature in Zhao's research ranges from 1200–1300 °C. At this temperature, a ⟨100⟩-fibre texture can be achieved. The selection of the solution treatment temperature is a critical issue; if the temperature is too low, the fibre texture will not form. Conversely, if the temperature is too high, there is a potential for microcracks to develop, which would adversely affect the superelastic properties. Choi *et al.* [19] introduced an alternative fabrication technique to cold rolling known as the in-rotating-water spinning (INROWASP) technique. The INROWASP technique can quickly produce long and continuous wire of the desired size without requiring additional hot or cold working. This technique aims to produce a bamboo-like crystal structure, known as an oligo-crystalline structure. These studies have contributed valuable insights into the fundamental properties of NCATB alloys and their potential as competitive shape-memory materials. Despite these advancements, significant limitations persist. One major issue is the inconsistency in superelastic values reported across different studies. In this case, Tseng, Zhang, and Zhao used similar experimental methodologies but obtained markedly different results, indicating potential variability in experimental conditions or alloy compositions. Likewise, results from other studies similar to Choi *et al.* also showed inconsistent outcomes despite using similar fabrication techniques [12, 19–22]. Moreover, much of the current research remains theoretical or simulation-based, with limited practical implementation. This gap between theoretical potential and real-world application is a critical barrier to the broader adoption of NCATB alloys.

To uncover the full potential of NCATB alloys, it is essential to explore key factors that influence their superelastic properties. By investigating these variables in more detail, researchers can gain a deeper understanding of the phenomena governing the behaviour of NCATB alloys. In this review, the aim is to address these research gaps by providing a comprehensive analysis of the factors affecting the superelastic properties of NCATB alloys. Detailed exploration of alloy design, fabrication methods, and heat treatment processes, will enhance the understanding and optimization of NCATB alloys, paving the way for their broader scientific and industrial applications. Additionally, this article will provide a foundational understanding and facilitate future research efforts by summarising the existing data and methodologies, thereby offering a comprehensive discussion of the collected research data organised according to the evolving research methodologies.

2. Shape-Memory Alloys

SMA is one type of smart materials first discovered by Olander in 1932 in the Au–Cd alloy [1]. In that alloy, Olander observed a phenomenon capable of remembering shapes and documented it in research reports using the term 'rubber-like effect' [5]. Over time, the terminology used to describe the shape-memory capability of SMA materials has evolved, including terms like shape recovery, superelasticity, and pseudo-elasticity, but fundamentally refers to the material's ability to return to its original shape after deformation under certain conditions [23–26]. Based on various discoveries, experts concluded that the main properties of SMA materials are superelasticity and shape-memory effect. The pinnacle of SMA material development occurred 30 years after the discovery of the SMA phenomenon in the Au–Cd alloy by Olander when a naval ordnance laboratory in America (Naval Ordnance Laboratory) accidentally discovered the SME phenomenon in fatigue test samples of equiatomic nickel–titanium (Ni–Ti) alloy when heated, later known as NiTinol [7, 26, 27]. The impact of this discovery led to a massive development of NiTi, which to this day remains one of the SMA products widely used in various industries [3, 6, 23, 28–31]. This has established the NiTi alloy as a benchmark in further research and development of SMA materials.

Research and development of SMA materials continue to produce competitive SMA products. Several alternative alloys have been introduced as candidates to substitute NiTi alloys, which are known to be relatively expensive in terms of both raw materials and fabrication complexity [6, 25, 32]. These alternative alloys include Fe and Cu-based SMAs, which have significant cost efficiency impacts. Apart from cost factors, Fe and Cu alloys also have other advantages such as abundant raw material availability [32–37]. Among these two types of SMA materials, Fe-based alloys have become a major topic of research and development [38–44]. One particularly notable Fe-based SMA is the Fe–Ni–Co–Al–Ta–B (NCATB) alloy, which has achieved a remarkable superelasticity value of 13.5%, nearly doubles that of NiTi, which is of 7.5% [11].

However, achieving the superelastic value of the NCATB alloy has raised several new issues. This value can be obtained through a relatively high deformation process reaching 98.6% and resulting in extremely thin samples of 0.2 mm thickness. Some researchers have pointed out that these conditions may pose challenges when applied in an industrial setting [12, 45]. Consequently, various fabrication methods are being explored to produce more universally applicable sample forms, aiming for broader application potential. The journey to develop new fabrication techniques for NCATB alloys has proven to be challenging. Many of the techniques attempted have not yet achieved the significant superelastic values reported by Tanaka. This discrepancy may be attributed to factors such as the spe-

cific alloy composition and the TMT schemes used. It highlights the need for further detailed research to refine fabrication methods and optimize the superelastic properties of NCATB alloys.

3. Fe-Based SMA

Fe-based SMA alloys are a type of material that combines superelastic properties similar to elastomers with strength comparable to titanium. This was revealed by Ma *et al.* in their study [46]. The study also highlights the potential of Fe-based alloys, noting their excellent shape recovery, high ductility, and damping capacity, making them suitable for various applications in both the medical field [14, 34, 47–52] and the construction industry [38, 40, 53–62]. Data on the potential of Fe-based alloys, in terms of superelastic properties and tensile strength, compared to various materials are summarized in Table 1.

Fe-based SMA materials can be classified into several groups based on their alloying elements, including FePd [15, 48, 49, 64, 65], FePt [48, 49], FeMn [21, 52, 66, 67] and FeNiCo [12, 20, 68–70]. In FePd and FePt alloys, the transformation mechanism involved is f.c.c.-austenite to b.c.t.-martensite [32, 41]. These alloys have not been extensively explored due to their drawbacks of high cost and the fact that they do not exhibit superelasticity at room temperature [40]. However, one study suggests that Fe–Pd alloys have the potential to be an alternative to Ni–Ti alloys for actuator applications in the medical field [15]. This study highlights three key advantages of Fe–Pd over NiTi. Firstly, contactless tissue stimulation: applying an external magnetic field to these materials can induce large, reversible changes in their shape (up to 5%) without needing direct physical contact. This can be used to stimulate tissue around implants, potentially promoting bone formation and improving fixation. Secondly, remote adjustment of implants: magnetic fields can be used to adjust the shape and functionality of implants (like stents and clamps) even after they are inserted, allowing for better fitting and performance. Thirdly, combining ferromagnetic shape memory with existing properties, these

Table 1. **Comparison of properties between Fe-based SMAs and different materials**

No	Materials	Stress limit, MPa	Recoverable strain, %	Ref.
1	Fe-based SMA (NCATB)	1200	13.5	[11]
2	Cu-based SMA	360	5	[63]
3	NiTi based SMA	≈550	7	[11]
4	Titanium alloys	≈1000	1	[46]
5	Elastomer	≈30	>10	[46]
6	Steel	≈1400	<0.5	[46]
7	Single wall CNT	≈3000	≅5	[46]

materials retain the beneficial properties of conventional shape-memory alloys, especially pseudo-elasticity (flexibility with low stiffness). This is valuable in medical applications as it reduces the stress shielding effect on bones. Additionally, miniaturization of this ferromagnetic shape-memory (FMSM) effect within magnetically controlled membranes opens the door for developing new medical devices of magnetically controlled stents, vena cava filters (used to prevent blood clots), abdominal aortic aneurysm devices (treating weakened areas in the aorta), and atrial septal defect occlusion devices (closing holes in the heart) [15, 65].

The FeMn alloy is one of the SMA materials that have been extensively researched because it has the best SME among all Fe alloys. The SME mechanism in FeMn alloys utilizes the f.c.c.-austenite to h.c.p.-martensite transformation [32, 41]. Additionally, FeMn alloys have a relatively wide transformation temperature window to exhibit shape-memory properties and good corrosion resistance, making them highly potential for application in various industrial fields [39, 67, 71]. However, FeMn alloys are referred to as semi-superelastic alloys because they do not achieve a balance between thermal driving force and elastic energy, resulting in a semi-thermoelastic martensitic condition [9, 32, 36]. In fact, some studies state that FeMn alloys do not possess superelastic properties [27, 40]. As research has progressed, it has been found that the factor contributing to thermoelastic martensite formation in FeMn alloys is the element Ni. In FeMnAlNi alloys, Ni plays a role in producing coherent *B*2 precipitates in the b.c.c. matrix [66].

Furthermore, the FeNiCo alloy has achieved the highest superelastic value in the history of SMA material research to date. This discovery was made by Tanaka *et al.* through their research on the polycrystalline alloy Fe–28Ni–17Co–11.5Al–2.5Ta–0.05B (at.%) known as NCATB [11]. In the NCATB alloy, the elastic energy and driving force energy reach equilibrium with the formation of coherent precipitates during the f.c.c.-austenite to b.c.t.-martensite phase transformation [9, 41]. With this equilibrium, the martensitic phase formed is thermoelastic, allowing reversible transformation. Other advantages of the NCATB alloy include the ability to exhibit superelastic properties at room temperature, although its transformation temperature window is not as wide as that of the FeMn alloy.

4. Superelasticity and Transformation Response

Superelasticity is the ability of SMA materials to return to their original shape, when the load is removed. This condition can occur under the requirement that the plastic deformation does not exceed the allowable limit; the temperature during plastic deformation is not higher than the temperature, at which martensite can be induced by loading, and when the load is released, the material can return to its original shape [9]. The su-

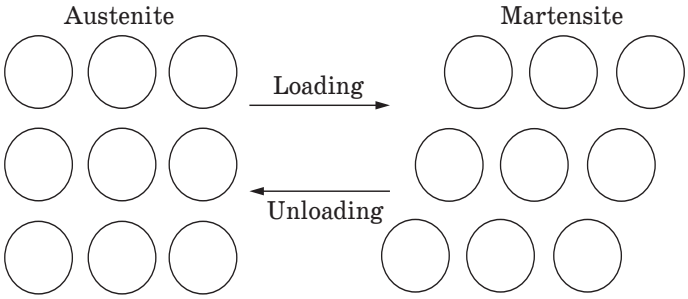

Fig. 1. Macroscopic illustration of superelastic mechanisms in SMA materials [44]

perelastic mechanism in NCATB alloys involves the reversible transformation between γ-f.c.c. and α′-b.c.t. [41]. When the SMA material is in the austenite condition under load, a phenomenon of stress-induced martensite occurs, driving the phase transformation from austenite to thermoelastic martensite. This transformation condition involves a driving force to generate dislocation, and simultaneously, coherent precipitates generate elastic energy to prevent deformation from entering the plastic region [9]. When the load is removed, the elastic energy is converted to energy to return the alloy to its parent phase. This reversible transformation mechanism involves volume changes and a relatively small hysteresis temperature ($T_h = A_f - M_s$). The schematic of this superelastic mechanism is illustrated in Fig. 1.

Table 2. **Effect of solution treatment and ageing on various NCATB alloys (here, n.a —**

No.	Composition	Sol. treatment, °C	Time, h	Ageing, °C
1	Fe–28Ni–17Co–11.5Al–2.5Ta–0.05B	1300	18	600
2	Fe–28Ni–17Co–11.5Al–2.5Ta	1300	24	n.a
3	Fe–28Ni–17Co–11.5Al–2.5Ta	1250	n.a	700
4	Fe–28Ni–17Co–11.5Al–2.5Ta–0.05B	1300	1	n.a
5	$Fe_{41}Ni_{28}Co_{17}Al_{11.5}Ta_{2.5}$	1300	24	700
6	Fe–28Ni–17Co–11.5Al–2.5Ta–0.05B	1315	20	n.a
7	$Fe_{50}Ni_{28}Co_{17}Al_{11.5}Ta_{2.5}$	1300	1	n.a
8	Fe–28Ni–17Co–11.5Al–2.5Ta–0.05B	1220	1	600
9	$Fe_{41}Ni_{28}Co_{17}Al_{11.5}Ta_{2.5}$	1300	1	600
10	Fe–28Ni–17Co–11.5Al–2.5Ta–0.05B	n.a	n.a	600
11	Fe–28.5Ni–17.5Co–11.5Al–2.5Ta–0.05B	1300	0.5	n.a
12	FeNiCoAlTaB	1300	1	600
13	$Fe_{41}Ni_{28}Co_{17}Al_{11.5}Ti_{2.5}$	1200–1300	0.5	n.a
14	Fe–30Ni–15Co–10Al–2.5Ti–0.05B	1200	3	n.a
15	FeNiCoAlTaB	n.a	n.a	800
16	Fe–28Ni–20Co–11.5Al–2.5Ta–0.05B	1300	1	600
17	$Fe_{60.5-x}Ni_{28}Al_{11.5}Ta_x$ (x = 0.5, 1, 1.5 at.%)	1280	0.5	700
18	$Fe_{41}Ni_{28}Co_{17}Al_{11.5}(Ti+Nb)_{2.5}$	1277	1	600
19	Fe–28Ni–17Co–11.5Al–2.5Nb–0.05B	1220	1	600

The primary factor influencing the SE properties of SMA materials is the presence of a thermoelastic (TE) martensite phase, which enables reversible transformation between austenite (f.c.c.) and martensite (b.c.t.) [34, 72–74]. The martensite phase in Fe-based SMA materials forms spontaneously during rapid cooling. As a result, the time required for the decomposition of austenite into ferrite and cementite through eutectoid diffusion is not met [9]. This reversible transformation phenomenon occurs when a load is applied to the material and then released. This type of martensite can only be obtained when the specified alloy design can promote the formation of coherent γ′-precipitates with respect to the parent matrix (γ-f.c.c.) [11]. Previous research explains that coherent γ′-precipitates in NCATB alloys consist of compounds between Ni, Fe, and Al forming (Ni, Fe, Co)$_3$(Al, Ta, Nb) [11, 41, 69, 73]. An illustration of coherent precipitates is outlined in **Fig. 2**.

The role of γ′-precipitates in producing TE martensite is by controlling the slip planes in the atomic matrix of a crystal structure during the transformation process [34]. This slip-plane control can occur because the precipitates have continuous and coherent connectivity with the matrix [75]. When the slip planes are controlled, equilibrium between the thermal driving force and elastic energy in the martensite phase will be achieved [41]. This condition is also influenced by the size of the γ′-precipitates. When the size is not proportional, it will lead to a reduction in SE proper-

not available in the paper; RT — room temperature)

Time, h	SE, %	SE temp., °C	M_s, °C	A_f, °C	γ′ size, nm	Ref.
72	13.5	RT	−86	−62	n.a	[11]
n.a	3.4	−26	−136 to −98	−91 to −63	n.a	[88]
7	6.8	−63	−113	−93	5	[33]
n.a	14.3	−196	n.a	n.a	3.06–6.49	[82]
1	4.5	−130	n.a	n.a	n.a	[92]
n.a	1.7	<0	n.a	n.a	5–8	[83]
n.a	15	−196	n.a	n.a	n.a	[89]
96	3.2	RT	n.a	n.a	n.a	[91]
90	0.25–0.7	<0	−108	−65	n.a	[93]
72	1.6	RT	n.a	n.a	n.a	[18]
n.a	2.5	n.a	n.a	n.a	n.a	[17]
72	7	RT	n.a	n.a	3–10	[19]
n.a	0.5	RT	n.a	n.a	n.a	[85]
n.a	4.2	RT	−35	−4	n.a	[84]
1	1.2	RT	n.a	n.a	n.a	[80]
72	1.3	RT	n.a	−94.15	4 ± 0.2	[70]
60	17	RT	n.a	n.a	n.a	[68]
48	1.6	RT	n.a	n.a	n.a	[13]
96	3.2	RT	−135	−130	n.a	[94]

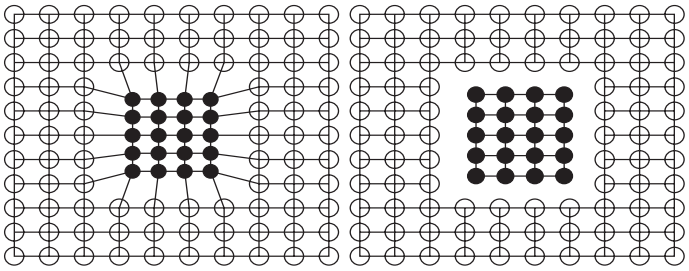

Fig. 2. Illustration of coherent (left) and incoherent (right) precipitates

ties or even the reversible transformation may not occur. According to previous research, the size of γ'-precipitates for producing TE martensite should not exceed 10 nm [41]. If any of these conditions are not met, the alloy will not exhibit superelastic properties.

5. The Influence of Alloying Elements

In addition to influencing the formation of coherent precipitates, the constituent elements in NCATB alloys have other important roles [9]. The element of Ni acts as an austenite stabilizer and is capable of producing thermoelastic martensitic transformation [11]. The element of Co contributes to increasing the matrix strength through solid solution strengthening and affects the increase in martensitic transformation temperature [11, 76, 77]. The element of Al plays a role in the formation of coherent precipitates and, in certain amounts, will cause a decrease in the austenite finish temperature and the hysteresis temperature [76]. Tantalum is the most effective element in increasing the γ' solvus temperature and hardness value during the ageing process [11, 76]. One of the elements used in the development of FeNiCo-based SMA materials is Ti. Titanium has a smaller atomic size compared to Ta. Due to its small size, Ti atoms will distribute more easily in the matrix and increase the ductility of the SMA material [72]. Additionally, Ti can also reduce the duration of the ageing process required to produce coherent precipitates [69]. Another study states that the use of Ti in the alloy provides several positive effects, including accelerating the precipitation process necessary for the desired superelastic response by maintaining a small precipitate size; Ti does not tend to form carbides, which could contribute to the reduction of the materials' mechanical properties; and Ti has a melting point that allows it to be homogeneously distributed during the heating process [78]. The element of B strengthens the grain boundaries of the alloy and prevents the formation of brittle grain boundary precipitates [41, 72, 79–83]. Therefore, the alloying elements control the strength and stability during the austenite-martensite phase transformation process in SMA alloys. However, systematic data on the alloy design rules are still limited. Thus, modifying alloy design remains an interesting topic for further study to find opportunities to improve SE properties.

As mentioned earlier, in addition to influencing the formation of coherent γ′-precipitates, alloying elements also prevent the formation of other undesirable precipitates such as β-precipitates. This type of precipitate tends to grow at high-angle grain boundaries (HAB), which are more vulnerable in polycrystalline materials compared to single-crystalline materials [17]. Previous research stated that β precipitates tend to grow in grains with angles > 15° [84]. Furthermore, the presence of β precipitates can reduce the mechanical properties of SMA materials because they are brittle and may initiate cracks at grain boundaries [17]. Other research also indicated that β precipitates hinder the grain growth in SMA materials, affecting the resulting superelastic properties [17, 85].

Due to the negative impact of β-precipitates, several preventive techniques need to be applied, one of which is the use of alloying elements. One alloying element proven to control the formation of β-precipitates is boron [11, 17, 80, 82]. Boron in SMA materials reduces the grain-boundary energy required for precipitate nucleation. Without this energy, precipitates find it difficult to grow.

6. Thermomechanical Process

The formation of coherent precipitates in alloy materials is not only determined by alloy design but also significantly influenced by the TMT process [70]. The thermomechanical treatment process consists of deformation and heating processes performed in stages, each contributing to the final properties of materials [73]. These process aims to achieve two primary objectives: first, the production of precipitates with specific distribution and size [79, 86]; second, the development of a texture with dominant orientations and planes [18, 83, 87]. Understanding the TMT process is crucial for optimizing the performance and characteristics of advanced alloy systems.

Various studies have revealed that achieving optimal SE values in NCATB alloys requires obtaining a strong texture with $\{035\}\langle 100\rangle$ orientation through the TMT process [11, 17, 18, 70, 82]. When SMA materials have a strong texture, the dislocation density in the grains will be reduced, facilitating the migration of phase interfaces during the thermoelastic transformation process [9]. A study indicates that when the material is rolled with deformation less than 90%, the grains exhibit random orientations without a dominant direction, thus failing to manifest superelastic properties [9, 84]. However, when the deformation percentage increases to 98.5%, the dominance of crystals in the $\langle 100\rangle$ orientation aligned with the rolling direction becomes significant, resulting in SE properties. There is also a differing viewpoint that suggests the optimal solution treatment temperature is crucial for generating the desired texture without needing deformation of above 98% [85]. However, texture orientation alone does not solely determine superelastic properties. Another study has

found a strong correlation between texture and precipitates in achieving superelasticity. If a material has a proportional texture but lacks adequately sized precipitates, the superelastic value will decrease [79]. Further, other research indicates that the primary factor influencing superelasticity is the strain glass transition caused by dense precipitates [68]. Superelasticity is derived from stress or grain boundary defects due to strain glass, inducing phase transformation.

The thermomechanical treatment process is a key factor in the formation of coherent precipitates and the development of desirable material properties in alloy systems [70, 73]. The precise control of deformation and heating stages enables the production of alloys with specific precipitate distributions and textures [9, 79]. The significant impact of deformation percentage on texture orientation and superelastic properties highlights the delicate balance required in the TMT process [70]. Because of that, further research is needed to explore the effects of minor variations in the TMT parameters, which could lead to advancements in the performance and application of high-performance alloys like NCATB. Understanding and optimizing the TMT process will continue to be a critical area of study in materials science.

7. The Influence of Heat Treatment on Superelastic Properties

As previously explained, in addition to deformation mechanisms, heat-treatment mechanisms in the TMT process are aimed to achieve matrix uniformity, grain size, and coherent precipitate formation. Generally, heat treatment processes in the fabrication of shape-memory alloys consist of solution treatment and ageing processes. The solution treatment has several objectives, including producing a primary austenite (γ) matrix by dissolving saturated elements and controlling texture recrystallization through grain size [11, 16, 18].

Zhao *et al.* [18] investigated variations in solution treatment temperatures 1150, 1200, 1250, and 1300 °C. Their results showed that solution treatment at a minimum temperature of 1250°C yielded the most optimal superelastic properties. This was evidenced by strong ⟨100⟩ texture orientation and the formation of a single-phase austenite (γ) matrix when heated at 1250–1300 °C. Zhao *et al.* also stated that solution treatment affects the formation of intermetallic phases. When heated at 1200 °C, XRD analysis indicated that the remaining intermetallic phases were only NiAl and Co_3Ta, while other intermetallics like Ni_3Ta, Al_3Ta, and Al_3Fe dissolved completely. Zhao *et al.* also found that temperatures above 1300 °C could potentially cause microcracks, negatively influencing superelastic properties. Zhao concluded that the holding time of the solution treatment process does not significantly affect superelastic values. Contrary to Zhao *et al.*, Tseng *et al.* [16] stated different opinions regarding the duration of

solution treatment for NCATB alloys. In their work, the duration of the solution treatment was varied at 1250 °C for 0.5 and 1 hour. They found that duration of 1 hour provided several benefits, including increasing grain size, which reduces the formation of triple junctions as areas where brittle precipitates form, thus enhancing superelastic properties. This was quantitatively proven, with the proportion of low angle boundaries (LAB) increasing from 15.4% to 39.5% in samples treated for 1 hour. Effects of heat treatment on various NCATB alloys are tabulated in Table 2.

The ageing process plays a crucial role in forming precipitates within the austenite matrix [17, 79, 81, 88, 89]. Previous research has indicated that coherent nanosize precipitates are obtained through the ageing process. The formation of these coherent precipitates strengthens the austenite matrix, thus controlling plastic deformation through dislocation slip during the martensitic transformation process [69]. When this condition is met, reversible austenite-martensite transformations can occur. Variables affecting the aging process include temperature and holding time. Tanaka's research mentioned that the proportional temperature and holding time to achieve low hysteresis temperature ($T_{\text{hyst}} = A_{\text{f}} - M_{\text{s}}$) and high hardness are 600 °C with a minimum holding time of 40 hours [11]. As the aging temperature increases, hardness also increases. Changes in hardness will influence the martensitic-transformation temperature [88, 90]. Hardness will reach saturation points at 650 and 700°C, where increased hardness is directly proportional to increased hysteresis temperature. This anomaly is due to the growth in size of γ′-precipitates at these temperatures (20 nm), affecting coherence and leading to increased austenite finish temperature (A_f) [79, 90]. Additionally, the loss of coherence is caused by the excessive growth of β-precipitates, which negatively affects mechanical properties [90].

8. Fabrication Techniques for NCATB

8.1. Cold Rolling

Various efforts to modify the microstructure have been made to achieve textures with dominant orientations. As previously explained, cold rolling with very high deformation (≈99%) remains one of the most widely used manufacturing methods for polycrystalline NCATB materials [11, 16, 18, 41, 91]. This deformation leads to the formation of specific dominant texture orientations capable of producing superelastic properties. However, as a consequence, samples processed through high-deformation cold rolling result in extremely thin sheets (0.2 mm), limiting their industrial application.

One of the researchers who achieved a high superelastic value of 13.5% at room temperature is Tanaka [11]. In Tanaka's study, the cold rolling fabrication technique was performed stepwise, reaching a deforma-

tion percentage of 98.6% without intermediate annealing. This process resulted in a texture characteristic dominated by the {035}⟨100⟩ direction and plane. Additionally, Tanaka achieved a tensile strength of 1200 MPa in the NCATB alloy. In another study, Zhaoxia *et al.* [68] attempted a different approach to achieve superelasticity without high deformation rolling. Zhaoxia stated that superelastic properties are not always produced through the dominance of a specific texture; instead, a critical factor is the presence of densely packed precipitates. The dense precipitates enable superelasticity through strain-induced transformation, originating from the transition of strain glass to martensite. Various studies with their respective achievements in generating superelastic properties of NCATB alloys are summarized in Table 3.

8.2. Wire Drawing

Because of the high deformation rolling process, the NCATB samples have extremely thin dimensions. This condition poses limitations for industrial applications. Therefore, alternative fabrication methods are necessary, one of which is via wire fabrication. Choi *et al.* [19] conducted NCATB wire fabrication using the in-rotating-water-spinning (INROWASP) method, where molten metal from the induction process is cooled through a rotating water drum, producing wire-like products with a structure similar to single crystals (oligo-crystalline). This process achieved SE values of 7%, despite not showing texture in specific planes and directions (untextured). The drawbacks of this process include its complexity, high cost, and limited material quantity that can be processed, making it unsuitable for mass production [12].

Choi *et al.* [19] have also conducted NCATB fabrication using the INROWASP technique to demonstrate that shape-memory properties can be achieved without requiring a crystallographic texture. Through the INROWASP technique, Choi aimed to minimize grain constraints and intergranular precipitation by achieving an oligo-crystalline structure. By minimizing grain constraints, the mechanical properties of the material were expected to improve. The oligo-crystalline structure helps reduce these constraints because it has a lower total grain boundary area compared to a polycrystalline structure. With fewer grain boundaries, the physical barriers posed by these boundaries are reduced. Furthermore, intergranular precipitation refers to the formation of small particles along grain boundaries, which can cause brittleness and reduce the mechanical properties of the material. By reducing the total grain boundary area through the oligo-crystalline structure, the likelihood of precipitation at grain boundaries is also minimized. This helps maintain the structural integrity and mechanical properties of the material. Some information regarding the characteristics produced through wire fabrication techniques of NCATB alloys and others can be observed in Table 4.

Table 3. **Various deformation percentages in cold rolling fabrication processes and the resulting characteristics (n.a — not available in the paper)**

No.	Composition	Crystal structure	Deformation, %	SE, %	Texture	Tensile, MPa	grain size, μm	γ′ size, nm	Ref.
1	Fe–28Ni–17Co–11.5Al–2.5Ta–0.05B	Poly	98.6	13.5	{035} ⟨100⟩	1200	400	n.a	[11]
2	Fe–28Ni–17Co–11.5Al–2.5Ta	Poly	90	n.a	n.a	n.a	n.a	n.a	[76]
3	Fe–28Ni–17Co–11.5Al–2.5Ta–0.05B	Single	98.5	3.2	⟨100⟩	960	n.a	n.a	[91]
4	$Fe_{41}Ni_{28}Co_{17}Al_{11.5}Ta_{2.5}$	Poly	93	0.25–0.7	⟨100⟩	n.a	n.a	n.a	[93]
5	Fe–28Ni–17Co–11.5Al–2.5Ta–0.05B	Poly	98.5	1.6	⟨100⟩	n.a	n.a	n.a	[18]
6	Fe–28.5Ni–17.5Co–11.5Al–2.5Ta–0.05B	Poly	97.2	2.5	⟨100⟩	1000	n.a	n.a	[17]
7	$Fe_{41}Ni_{28}Co_{17}Al_{11.5}Ti_{2.5}$	Poly	90	0.5	{230} ⟨100⟩	550	3–10	n.a	[85]
8	Fe–30Ni–15Co–10Al–2.5Ti–0.05B	Poly	98.5	4.2	{012} ⟨100⟩	n.a	n.a	n.a	[84]
9	Fe–28Ni–20Co–11.5Al–2.5Ta–0.05B	Poly	98.8	1.3	{001} ⟨110⟩	n.a	128	4 ± 0.2	[70]
10	Fe–28Ni–17Co–11.5Al–2.5Ta–0.05B	Poly	98.6	n.a	n.a	n.a	n.a	n.a	[79]
11	$Fe_{60.5-x}Ni_{28}Al_{11.}5Ta_x$ (x = 0.5, 1, 1.5%)	Poly	42.9	17	n.a	n.a	n.a	n.a	[68]
12	$Fe_{40.95}Ni_{28}Co_{17}Al_{11.5}Ta_{2.5}B_{0.05}$	Poly	97	1; 2.6	⟨110⟩	765; 560	210; 1570	10; 16	[16]
13	$Fe_{41}Ni_{28}Co_{17}Al_{11.5}(Ti+Nb)_{2.5}$	Poly	97	1.6	n.a	n.a	n.a	n.a	[13]
14	Fe–28Ni–17Co–11.5Al–2.5Nb–0.05B	Poly	98.5	3.2	⟨001⟩	n.a	n.a	n.a	[94]

Table 4. **Development of fabrication techniques for NCATB and other alloys (n.a — not available in the paper; VIM — vacuum induction melting; INROWASP — in rotating water spinning)**

No.	Composition	Melting method	Crystal	Metal working	Deformation, %	SE, %	Texture	Tensile, MPa	grain size, μm	γ′ size, nm	Ref.
1	FeNiCoAlTa	INROWASP	Oligo	directional solidification	n.a	7	untextured	1200	n.a	3–10	[19]
2	$Fe_{43.5}Mn_{34}Al_{15}Ni_{7.5}$	VIM	Poly	cold drawn	75	6.7	[110]	600	n.a	n.a	[21]
3	FeNiCoAlTaB	INROWASP	Oligo	directional solidification	91.35	1.2	n.a	n.a	n.a	n.a	[80]
4	$Fe_{41}Ni_{28}Co_{17}Al_{11.5}Ti_{2.5}B_{0.05}$	VIM	Poly	cold drawn	98.65	n.a	{110} ⟨111⟩	n.a	<10	2; 8	[12]
5	Fe–8Mn–5Si–13Cr–6Ni–12Co	VIM	Poly	cold drawn	57	n.a	n.a	n.a	n.a	n.a	[95]
6	Fe–34Mn–15Al–7.5Ni	VIM	Poly	cold drawn	88.9; 75	5.5	⟨110⟩	325	433	n.a	[22]

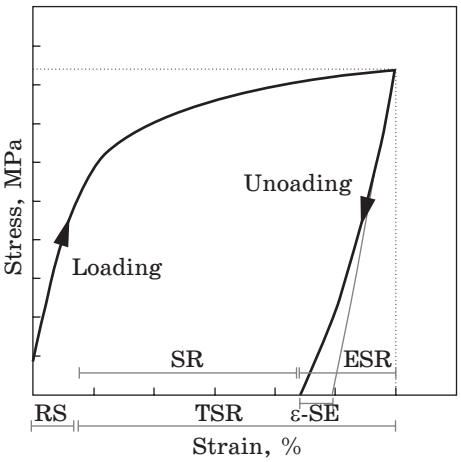

Fig. 3. The stress–strain superelastic recovery values (ε-SE)

In their work, Sobrero *et al.* [12] performed wire fabrication for SMA with FeNiCoAlTiB alloy using conventional method. The process began with homogenizing rod-shaped samples obtained from vacuum arc melting at 1150 °C for 4 hours. Subsequently, wire fabrication was conducted in stages, with a total deformation of 98.6%, similar to Tanaka's method. Through this process, Sobrero achieved SE values of 1.3% with texture orientation in the {110} ⟨111⟩/⟨001⟩ direction. Omori *et al.* and Ozcan *et al.* conducted wire fabrication for FeMnAl alloys. They achieved SE values of 5% and 6.7%, respectively [21, 22]. The main difference in the TMT schemes between Omori and Ozcan lies in microstructure modification. Besides wire fabrication, Ozcan also implemented heat treatment modifications to produce abnormal grain growth. Abnormal grains are expected to reduce the occurrence of triple junctions in the resulting microstructure, thereby helping to reduce the formation of undesirable precipitates and enhancing SE values [9, 21, 66]. Andrade *et al.* conducted wire fabrication for Fe–Mn–Si–Cr–Ni–Co alloys. The total deformation involved in wire fabrication was of 57%, with two heat treatments [95]. This process achieved a total shape recovery (TSR) of 83%. TSR is the total amount of elastic shape recovery (ESR), shape recovery (SR), and residual strain (RS). The tensile testing scheme for SMA materials is shown in Fig. 3.

9. Recent Application Development

The development of applications for NCATB SMA in various industrial fields has not been as extensive compared to other alloys. Given its various advantages, NCATB should have the same opportunities as other alloys. According to the reviewed literature, discussions on NCATB applications mainly focus on damper or earthquake-damping materials [59–62]. This is due to NCATB's superior damping capacity of 81 MJ/m^3 compared to other alloys like NiTi-based and Cu-based alloys [96, 97], which have damping capacities of 16 MJ/m^3 and 38 MJ/m^3, respectively [11], [41]. In their research, Zheng *et al.* [98] found that SMA materials play a crucial role in earthquake-damping applications to enhance the re-centring capacity and energy dissipation of bridge structures. By integrating SMA into seismic isolators such as friction pendulums and flat sliding bearings, the

study demonstrated the significant potential of SMA materials in improving sustainable adaptability and seismic resilience.

Dezfuli *et al.* [61, 62] attempted to develop earthquake damper materials known as CFR-HDRB (Carbon Fibre Reinforced High Damping Rubber Bearings). In their work, they evaluated the influence of the rubber bearing aspect ratio, SMA wire thickness, alloy type, and the amount of pre-strain on the SMA wire on the device performance when subjected to vertical pressure and cyclic lateral displacement in a specific direction. The simulation results indicated that incorporating SMA materials into HDRB enhanced damping by up to 38%. Bhowmick *et al.* [59] also reported similar findings, stating that NCATB alloy used in SMA-based friction bearing isolation systems (S-FBI) exhibited superior performance in mitigating seismic response. This was evidenced by the simulation results of S-FBI performance, which were conducted through nonlinear dynamic analysis under a series of recorded ground motions. The results demonstrated improved isolation efficiency and a reduction in peak displacement, ensuring that structures remain safe and stable during and after an earthquake. In another study, Habieb *et al.* [60] developed a hybrid isolation system consisting of Unbonded Fibre-Reinforced Elastomeric Isolator (UFREI) and SMA wire as an additional dissipative device to isolate a historic brick church. The analysis results indicated that significant damage to the base model of the church could be substantially reduced through the application of this isolation system. During earthquakes with strong amplitudes, the UFREI+SMA wire model exhibited the largest reduction in horizontal displacement and significantly mitigated damage, reducing the level of collapse to minor damage, owing to the high energy-dissipation capacity of SMA.

The potential of NCATB SMA in various industrial applications, particularly in earthquake damping, is evident through numerous studies. Despite its advantages, the adoption of NCATB SMA has not been as widespread as other alloys, highlighting a significant opportunity for further exploration and development. The superior damping capacity of NCATB alloys compared to other materials makes it an excellent candidate for seismic applications. Research has consistently shown that the integration of SMA materials, including NCATB, into seismic isolation systems can significantly enhance energy dissipation, re-centring capacity, and overall seismic resilience. However, current research on NCATB applications is primarily focused on potential and simulation studies, indicating a gap in practical, real-world implementations. This limited scope of research highlights the need for experimental validation and broader industrial usage. Expanding the research and development of NCATB SMA, applications could lead to more widespread utilization in various sectors, maximizing its advantages and improving structural safety and stability. Addressing this gap will require targeted efforts to demonstrate the versatility and

effectiveness of NCATB in a broader range of industrial contexts, moving beyond simulations to practical applications.

10. Potential Directions for Future Research

The advancements in the fabrication and processing techniques for Fe-based SMAs, particularly polycrystalline Fe–Ni–Co–Al–Ta–B (NCATB) alloys, have opened up new opportunity for further research. Despite significant progress, several challenges remain that future studies must address to fully realize the potential of these materials in various industrial applications. The following areas are key ones for future research that builds upon the existing knowledge.

10.1. Optimizing Fabrication Techniques

The fabrication techniques for NCATB alloys have shown promising results, yet each method presents unique challenges that limit their scalability and practical application. For instance, cold rolling, a widely used method, has achieved impressive superelasticity values but results in extremely thin sheets (≈0.2 mm), which constrain their industrial use. Exploring alternatives to cold rolling, such as wire drawing and the INROWASP technique, could open up new possibilities for larger-scale production while maintaining desirable mechanical properties. However, these methods, like the INROWASP technique used by Choi *et al.* [19], are complex and costly, limiting their feasibility for mass production. On the other hand, wire fabrication presents a viable alternative to thin sheet production, offering potential for broader applications. Studies by Sobrero *et al.* [12] and others have demonstrated the feasibility of achieving superelastic properties in NCATB wire using conventional wiredrawing methods. However, the superelasticity achieved in these studies remains relatively low compared to sheet fabrication methods. Future research should explore the optimization of wire fabrication processes, such as improving the control of abnormal grain growth, as investigated by Ozcan *et al.* [21, 22], while also refining these processes to make them more efficient and scalable, perhaps by integrating hybrid techniques or developing new, more cost-effective methods.

10.2. Optimizing Microstructure and Precipitate Control

Achieving the optimal microstructure is crucial for improving the superelastic properties of NCATB alloys. Cold rolling processes have demonstrated the importance of creating dominant texture orientations, as shown by Tanaka *et al.* [11], which achieved a superelasticity value of 13.5%. However, recent studies, such as those by Zhaoxia *et al.* [68], have suggested that superelasticity can also be influenced by the presence of densely packed precipitates rather than specific texture dominance. Ad-

ditionally, detailed exploration into controlling the formation of β- and Ta-precipitates at grain boundaries, as reported by Zhang *et al.* [17], is critical for enhancing the performance of NCATB alloys. While optimizing the microstructure is fundamental to enhancing superelasticity, the importance of thermo-mechanical treatment processes cannot be disregard. TMT plays a complementary role in refining the mechanical properties of NCATB alloys, as demonstrated by Tseng *et al.* [16], where even minor variations in solution treatment influenced grain growth and superelasticity. Future research should therefore delve deeper into the TMT processes, such as recrystallization, phase transformation kinetics, and the influence of cooling rates. Establishing precise TMT process that ensure reproducibility and maximize the mechanical performance will be essential for the broader adoption of NCATB alloys in industrial applications. By integrating advanced microstructural control with optimized TMT techniques, researchers can unlock the full potential of NCATB alloys, paving the way for their use in more diverse and demanding environments.

10.3. Long-Term Performance and Durability

While studies such as those by Dezfuli *et al.* [61, 62] and Bhowmick *et al.* [59] have shown the promise of NCATB alloys in seismic damping systems, the long-term performance of these alloys under cyclic loading and extreme-temperature conditions remains underexplored. For NCATB alloys to be viable in demanding industrial environments, it is crucial to conduct extensive durability and fatigue tests. Investigating the degradation mechanisms, such as how environmental factors like oxidation, corrosion, and temperature fluctuations affect the long-term reliability of NCATB alloys, is essential. These studies will ensure that NCATB alloys maintain their superelastic and damping properties over extended periods, thereby solidifying their suitability for critical applications, such as earthquake damping and beyond.

10.4. Bridging the Gap between Simulations and Real-World Applications

While NCATB alloys have shown great promise in seismic isolation systems, as demonstrated by Dezfuli *et al.* [61, 62] and Bhowmick *et al.* [59], their potential applications extend far beyond earthquake damping. This current research remains confined to theoretical models and simulations, with limited real-world application. One of the critical challenges identified is translating the promising simulation results into tangible, practical applications. Future research should prioritize experimental validation of these simulation models, particularly in earthquake damping and other structural applications. Collaborating with industry partners to test NCATB-based damping systems in real-world scenarios, such as in bridge and building constructions, will be crucial for assessing the practical via-

bility of these materials. Beyond structural applications, future research should also explore other fields where the superior damping capacity and superelasticity of NCATB alloys could offer significant advantages. Industries such as aerospace, biomedical, and automotive could benefit greatly from these properties. By identifying and developing NCATB applications in these sectors, researchers can diversify the use of Fe-based SMAs and drive innovation across various technological domains.

By addressing these research directions, the scientific community can further unlock the potential of NCATB alloys, ensuring they become a competitive and widely adopted material in various industries. The path forward involves a combination of theoretical advancements, experimental validation, and practical application to overcome the current limitations and drive the future development of Fe-based shape-memory alloys.

11. Conclusion

Despite the significant potential and promising results achieved in research, the development of NCATB alloys has not been as extensive as other SMA materials. This is reflected in the limited number of specific journals addressing the shape-memory properties of NCATB alloys. Moreover, discussions on the application of NCATB alloys are mostly confined to their potential and simulations, without extensive practical implementation. Furthermore, studies by various researchers have shown inconsistencies in obtaining data, particularly superelastic values, even when using the same methodologies. This indicates that there are still many research gaps that need to be explored in more detail. Key factors affecting the superelastic properties of NCATB alloys are not yet fully understood, presenting numerous opportunities for further investigation. Some of the key variables that can be further elaborated to uncover the phenomena of superelasticity in NCATB alloys include alloy design, fabrication techniques, and heat treatment processes. The exploration of these factors could significantly enhance the understanding and optimization of NCATB alloys for both scientific and industrial applications.

Acknowledgements. The first author expresses his deep gratitude for the scholarship provided by the Research Centre for Metallurgy of the National Research and Innovation Agency.

REFERENCES

1. L. Lecce and A. Concilio, *Shape Memory Alloy Engineering for Aerospace, Structural and Biomedical Applications* (Vienna: Elsevier Ltd: 1996), p. 1–68; https://doi.org/10.1007/978-3-7091-4348-3_1
2. D.G. Poitout, *Biomechanics and Biomaterials in Orthopedics. 2nd ed.* (London: Springer: 2016); https://doi.org/10.1007/978-1-84882-664-9

3. S. Parvizi, S.M. Hashemi, and S. Moein, NiTi shape memory alloys: properties, *Nickel-Titanium Smart Hybrid Materials* (Elsevier: 2022), Ch. 19, p. 399; https://doi.org/10.1016/B978-0-323-91173-3.00021-3
4. K. Mehta and K. Gupta, Fabrication and Processing of Shape Memory Alloys, *SpringerBriefs in Applied Sciences and Technology* (Cham, Switzerland: Springer: 2019); https://doi.org/10.1007/978-3-319-99307-2
5. C. Lexcellent, *Shape-Memory Alloys Handbook* (London: Wiley: 2013); https://doi.org/10.1002/9781118577776
6. X. Chen, K. Liu, W. Guo, N. Gangil, A.N. Siddiquee, and S. Konovalov, *Rapid Prototyp. J.*, **25**, No. 8: 1421 (2019); https://doi.org/10.1108/RPJ-11-2018-0292
7. S.K. Patel, B. Behera, B. Swain, R. Roshan, D. Sahoo, and A. Behera, *Mater. Today Proc.*, **33**, No. 8: 5548 (2020); https://doi.org/10.1016/j.matpr.2020.03.538
8. J. Xia, Y. Noguchi, X. Xu, T. Odaira, Y. Kimura, M. Nagasako, T. Omori, and R. Kainuma, *Science*, **369**, No. 6505: 855 (2020); https://doi.org/10.1126/science.abc1590
9. Z. Li, Y. Zhang, K. Dong, and Z. Zhang, *Crystals*, **12**, No. 5: 602 (2022); https://doi.org/10.3390/cryst12050602
10. R.A. Rahman, D. Juhre, and T. Halle, *Pakistan J. Enginnering Appl. Sci.*, **24**, No. 5: 32 (2019).
11. Y. Tanaka, Y. Himuro, R. Kainuma, Y. Sutou, T. Omori, and K. Ishida, *Science*, **327**, No. 5972: 1488 (2010); https://doi.org/10.1126/science.1183169
12. C. Sobrero, V. Remich, J. Cassineiro, M.F. Giordana, G. Abreu Faria, A. Liehr, J. Freudenberger, T. Niendorf, and P. Krooß, *Shape Mem. Superelasticity*, **9**, No. 3: 531 (2023); https://doi.org/10.1007/s40830-023-00449-7
13. L.-W. Tseng, C.-H. Chen, W.-C. Chen, Y. Cheng, and N.-H. Lu, *Crystals*, **11**, No. 10: 1253 (2021); https://doi.org/10.3390/cryst11101253
14. J. Fiocchi, J.N. Lemke, S. Zilio, C.A. Biffi, A. Coda, and A. Tuissi, *Mater. Today Commun.*, **27**: 102447 (2021); https://doi.org/10.1016/j.mtcomm.2021.102447
15. U. Allenstein, Y.Ma, A. Arabi-Hashemi, M. Zink, and S.G. Mayr, *Acta Biomater.*, **9**, No. 3: 5845 (2013); https://doi.org/10.1016/j.actbio.2012.10.040
16. L. Tseng, M. Song, W.-C. Chen, Y. Hsu, and C. Chen, *Metals*, **14**, No. 6: 643 (2024); https://doi.org/10.3390/met14060643
17. C. Zhang, C. Zhu, S. Shin, L. Casalena, and K. Vecchio, *Mater. Sci. Eng. A*, **743**: 372 (2018); https://doi.org/10.1016/j.msea.2018.11.077
18. H. Zhao, H. Fu, J. Xie, and Z. Zhang, *Mater. Res. Express*, **5**, No. 1: 016508 (2018); https://doi.org/10.1088/2053-1591/aaa1fd
19. W.S. Choi, E.L. Pang, P.P. Choi, and C.A. Schuh, *Scr. Mater.*, **188**: 1 (2020); https://doi.org/10.1016/j.scriptamat.2020.06.067
20. J. Cassinerio, M.F. Giordana, E. Zelaya, V. Remich, P. Krooß, J. Freudenberger, T. Niendorf, and C. E. Sobrero, *Shape Mem. Superelasticity*, **10**, No. 1: 37 (2024); https://doi.org/10.1007/s40830-023-00470-w

21. H. Ozcan, J. Ma, S.J. Wang, I. Karaman, Y. Chumlyakov, J. Brown, and R.D. Noebe, *Scr. Mater.*, **134**: 66 (2017); https://doi.org/10.1016/j.scriptamat.2017.02.023
22. T. Omori, M. Okano, and R. Kainuma, *APL Mater.*, **1**, No. 3: 032103 (2013); https://doi.org/10.1063/1.4820429
23. J. Mohd Jani, M. Leary, A. Subic, and M.A. Gibson, *Mater. Des.*, **56**: 1078 (2014); https://doi.org/10.1016/j.matdes.2013.11.084
24. S. Barbarino, E.L. Saavedra Flores, R.M. Ajaj, I. Dayyani, and M.I. Friswell, *Smart Mater. Struct.*, **23**, No. 6: 063001 (2014); https://doi.org/10.1088/0964-1726/23/6/063001
25. P.S. Lobo, J. Almeida, and L. Guerreiro, *Procedia Eng.*, **114**: 776 (2015); https://doi.org/10.1016/j.proeng.2015.08.025
26. D. Patil and G. Song, *Smart Mater. Struct.*, **26**, No. 9: 1 (2017); https://doi.org/10.1088/1361-665X/aa7706
27. Z. Wang and A.M. Korsunsky, *Encycl. Smart Mater.*, **4**: 239 (2022); https://doi.org/10.1016/B978-0-12-803581-8.11793-X
28. R.E. McMahon, J. Ma, S.V. Verkhoturov, D. Munoz-Pinto, I. Karaman, F. Rubitschek, H.J. Maier, and M.S. Hahn, *Acta Biomater.*, **8**, No. 7: 2863 (2012); https://doi.org/10.1016/j.actbio.2012.03.034
29. A. Weirich and B. Kuhlenkotter, *Actuators*, **8**, No. 3: 61 (2019); https://doi.org/10.3390/act8030061
30. S. Jayachandran, K. Akash, S.S. Mani Prabu, M. Manikandan, M. Muralidharan, A. Brolin, and I.A. Palani, *Compos. Part B: Eng.*, **176**, No. 1: 107182 (2019); https://doi.org/10.1016/j.compositesb.2019.107182
31. N. Shayesteh Moghaddam, S. Saedi, A. Amerinatanzi, A. Hinojos, A. Ramazani, J. Kundin, M.J. Mills, H. Karaca, and M. Elahinia, *Sci. Rep.*, **9**, No. 1: 1 (2019); https://doi.org/10.1038/s41598-018-36641-4
32. K.K. Alaneme and E.A. Okotete, *Eng. Sci. Technol. Int. J.*, **19**, No. 3: 1582 (2016); https://doi.org/10.1016/j.jestch.2016.05.010
33. I.V. Kireeva, Y.I. Chumlyakov, V.A. Kirillov, I. Karaman, and E. Cesari, *Tech. Phys. Lett.*, **37**, No. 5: 487 (2011); https://doi.org/10.1134/S1063785011050221
34. I. Darwin Immanuel, M. Gangaraju, D. Arulkirubakaran, R. Malkiya Rasalin Prince, T. Debnath, and D. Palanisamy, *Mater. Today Proc.*, **68**, No. 5: 1718 (2022); https://doi.org/10.1016/j.matpr.2022.09.194
35. E.M. Mazzer, M.R. da Silva, and P. Gargarella, *J. Mater. Res.*, **37**, No. 1: 162 (2022); https://doi.org/10.1557/s43578-021-00444-7
36. S. Saedi, E. Acar, H. Raji, S.E. Saghaian, and M. Mirsayar, *J. Alloys Compd.*, **956**: 170286 (2023); https://doi.org/10.1016/j.jallcom.2023.170286
37. K.K. Alaneme, E.A. Okotete, and J.U. Anaele, *J. Build. Eng.*, **22**: 22 (2019); https://doi.org/10.1016/j.jobe.2018.11.014
38. Z.-X. Zhang, J. Zhang, H. Wu, Y. Ji, and D.D. Kumar, *Materials*, **15**, No. 5: 1723 (2022); https://doi.org/10.3390/ma15051723
39. T. Omori, K. Ando, M. Okano, X. Xu, Y. Tanaka, I. Ohnuma, R. Kainuma, and K. Ishida, *Science*, **333**, No. 6038: 68 (2011); https://doi.org/10.1126/science.1202232
40. A. Cladera, B. Weber, C. Leinenbach, C. Czaderski, M. Shahverdi, and M. Motavalli, *Constr. Build. Mater.*, **63**: 281 (2014); https://doi.org/10.1016/j.conbuildmat.2014.04.032

41. X. Wang, Y. Zhang, Z. Zhang, L. Liu, B. Wang, Y. Cui, I. Baker, and J. Cheng, *Crit. Rev. Solid State Mater. Sci.*, **49**, No. 2: 308 (2023); https://doi.org/10.1080/10408436.2023.2175641
42. F.C. Nascimento Borges, Iron based shape memory alloys: mechanical and structural properties, *Shape Memory Alloys — Processing, Characterization and Applications* (2013); https://doi.org/10.5772/51877
43. R.A. Ur Rahman, D. Juhre, and T. Halle, *Korean J. Mater. Res.*, **28**, No. 7: 381 (2018); https://doi.org/10.3740/MRSK.2018.28.7.381
44. M.Y. Hasbi, E. Mabruri, S.D. Yudanto, F.M. Ridlo, B. Adjiantoro, D. Irawan, I.G.P. Astawa, M.R. Rido, T.B. Romijarso, R. Roberto, D.P. Utama, and N. Amalia, *AIP Conf. Proc.*, **3003**, No. 1: 020054 (2024); https://doi.org/10.1063/5.0186259
45. D. Lee, T. Omori, K. Han, Y. Hayakawa, and R. Kainuma, *Shape Mem. Superelasticity*, **4**, No. 1: 102 (2018); https://doi.org/10.1007/s40830-018-0160-5
46. J. Ma and I. Karaman, *Science*, **327**, No. 5972: 1468 (2010); https://doi.org/10.1126/science.1186766
47. A. Francis, Y. Yang, S. Virtanen, and A.R. Boccaccini, *J. Mater. Sci. Mater. Med.*, **26**, No.3: 138 (2015); https://doi.org/10.1007/s10856-015-5473-8
48. Y. Wang, J. Venezuela, and M. Dargusch, *Biomaterials*, **279**: 121215 (2021); https://doi.org/10.1016/j.biomaterials.2021.121215
49. T. Huang, J. Cheng, and Y.F. Zheng, *Mater. Sci. Eng. C*, **35**, No. 1: 43 (2014); https://doi.org/10.1016/j.msec.2013.10.023
50. L.C. Trincă, L. Burtan, D. Mareci, B.M. Fernбndez-Pйrez, I. Stoleriu, T. Stanciu, S. Stanciu, C. Solcan, J. Izquierdo, and R.M. Souto, *Mater. Sci. Eng. C*, **118**: 111436 (2021); https://doi.org/10.1016/j.msec.2020.111436
51. B. Liu, Y.F. Zheng, and L. Ruan, *Mater. Lett.*, **65**, No. 3: 540 (2011); https://doi.org/10.1016/j.matlet.2010.10.068
52. A.M. Roman, V. Geantă, R. Cimpoeșu, C. Munteanu, N.M. Lohan, G. Zegan, E.R. Cernei, I. Ioniță, N. Cimpoeșu, and N. Ioanid, *Materials*, **15**, No. 2: 568 (2022); https://doi.org/10.3390/ma15020568
53. V.A. Silvestru, Z. Deng, J. Michels, L. Li, E. Ghafoori, and A. Taras, *Glas. Struct. Eng.*, **7**, No. 2: 187 (2022); https://doi.org/10.1007/s40940-022-00183-z
54. A. Muntasir Billah, J. Rahman, and Q. Zhang, *Structures*, **37**: 514 (2022); https://doi.org/10.1016/j.istruc.2022.01.034
55. M.R. Izadi, E. Ghafoori, M. Shahverdi, M. Motavalli, and S. Maalek, *Eng. Struct.*, **174**: 433 (2018); https://doi.org/10.1016/j.engstruct.2018.07.073
56. A. Hassanzadeh and S. Moradi, *Front. Struct. Civ. Eng.*, **16**, No. 3: 281 (2022); https://doi.org/10.1007/s11709-022-0807-3
57. C. Czaderski, M. Shahverdi, and J. Michels, *Constr. Build. Mater.*, **274**: 121793 (2021); https://doi.org/10.1016/j.conbuildmat.2020.121793
58. X. Qiang, L. Chen, and X. Jiang, *Materials*, **15**, No. 22: 8089 (2022); https://doi.org/10.3390/ma15228089
59. S. Bhowmick and S.K. Mishra, *Soil Dyn. Earthq. Eng.*, **100**: 34 (2017); https://doi.org/10.1016/j.soildyn.2017.03.037
60. A.B. Habieb, M. Valente, and G. Milani, *Eng. Struct.*, **196**: 109281 (2019); https://doi.org/10.1016/j.engstruct.2019.109281

61. F. Hedayati Dezfuli and M.S. Alam, *Eng. Struct.*, **61**: 166 (2014); https://doi.org/10.1016/j.engstruct.2014.01.008
62. F. Hedayati Dezfuli and M. Shahria Alam, *Smart Mater. Struct.*, **22**, No. 4: 045013 (2013); https://doi.org/10.1088/0964-1726/22/4/045013
63. C.D. Medina, R.A. Herrera, and J.F. Beltran, *Eng. Struct.*, **274**: 115151 (2023); https://doi.org/10.1016/j.engstruct.2022.115151
64. U. Allenstein, E.I. Wisotzki, C. Gräfe, J.H. Clement, Y. Liu, J. Schroers, and S.G. Mayr, *Mater. Des.*, **131**: 366 (2017); https://doi.org/10.1016/j.matdes.2017.06.032
65. M. Zink and S.G. Mayr, *Mater. Sci. Technol.*, **30**, No. 13: 1579 (2014); https://doi.org/10.1179/1743284714Y.0000000592
66. J. Xia, T. Hoshi, X. Xu, T. Omori, and R. Kainuma, *Shape Mem. Superelasticity*, **7**, No. 3: 402 (2021); https://doi.org/10.1007/s40830-021-00349-8
67. J.-M. Frenck, M. Vollmer, and T. Niendorf, *Mater. Lett.*, **365**: 136408 (2024); https://doi.org/10.1016/j.matlet.2024.136408
68. Z. Chen and W. Peng, *Funct. Mater. Lett.*, **13**, No. 01: 1950096 (2020); https://doi.org/10.1142/S1793604719500966
69. C. Lauhoff, V. Remich, M.F. Giordana, C. Sobrero, T. Niendorf, and P. Krooß, *J. Mater. Eng. Perform.*, **32**, No. 19: 8593 (2023); https://doi.org/10.1007/s11665-022-07745-w
70. X. Wang, Y. Zhang, Z. Zhang, J. Li, L. Liu, W. Jiang, and K. Du, *JOM*, **76**, No. 5: 2526 (2024); https://doi.org/10.1007/s11837-024-06469-7
71. N. Gangil, A.N. Siddiquee, and S. Maheshwari, *J. Manuf. Process.*, **59**: 205 (2020); https://doi.org/10.1016/j.jmapro.2020.09.048
72. Y.I. Chumlyakov, V. Kireeva, O.A. Kuts, Y.N. Platonova, V.V Poklonov, V. Kukshauzen, D.A. Kukshauzen, M.Y. Panchenko, and K.A. Reunova, *Russ. Phys. J.*, **58**, No. 11: 1549 (2016); https://doi.org/10.1007/s11182-016-0681-3
73. J. Ma, B.C. Hornbuckle, I. Karaman, G.B. Thompson, Z.P. Luo, and Y.I. Chumlyakov, *Acta Mater.*, **61**, No. 9: 3445 (2013); https://doi.org/10.1016/j.actamat.2013.02.036
74. N. Jost, *Mater. Sci. Forum*, **56–58**: 667 (1990); https://doi.org/10.4028/www.scientific.net/MSF.56-58.667
75. D.R. Askeland, P.P. Fulay, and W.J. Wright, *The Science and Engineering of Materials* (Stamford: CL-Engineering: 2011).
76. Y. Tanaka, R. Kainuma, T. Omori, and K. Ishida, *Mater. Today Proc.*, **2**, No. 3: S485 (2015); https://doi.org/10.1016/j.matpr.2015.07.333
77. T. Maki, K. Kobayashi, and I. Tamura, *J. Phys. Colloq.*, **43**, No. C4: 541 (1982); https://doi.org/10.1051/jphyscol:1982484
78. L.W. Tseng, J. Ma, I. Karaman, S.J. Wang, and Y.I. Chumlyakov, *Scr. Mater.*, **101**: 1 (2015); https://doi.org/10.1016/j.scriptamat.2014.12.021
79. Y. Geng, D. Lee, X. Xu, M. Nagasako, M. Jin, X. Jin, T. Omori, and R. Kainuma, *J. Alloys Compd.*, **628**: 287 (2015); https://doi.org/10.1016/j.jallcom.2014.12.172
80. F. Borza, N. Lupu, V. Dobrea, and H. Chiriac, *J. Appl. Phys.*, **117**, No. 17: 1 (2015); https://doi.org/10.1063/1.4917186

81. Y. Geng, M. Jin, W. Ren, W. Zhang, and X. Jin, *J. Alloys Compd.*, **577**: S631 (2013); https://doi.org/10.1016/j.jallcom.2012.03.033
82. M. Czerny, G. Cios, W. Maziarz, Y.I. Chumlyakov, N. Schell, and R. Chulist, *Mater. Des.*, **197**: 109225 (2021); https://doi.org/10.1016/j.matdes.2020.109225
83. H. Fu, W. Li, S. Song, Y. Jiang, and J. Xie, *J. Alloys Compd.*, **684**: 556 (2016); https://doi.org/10.1016/j.jallcom.2016.05.209
84. D. Lee, T. Omori, and R. Kainuma, *J. Alloys Compd.*, **617**: 120 (2014); https://doi.org/10.1016/j.jallcom.2014.07.136
85. C.E. Sobrero, C. Lauhoff, T. Wegener, T. Niendorf, and P. KrooB, *Shape Mem. Superelasticity*, **6**, No. 2: 191 (2020); https://doi.org/10.1007/s40830-020-00280-4
86. A. Wyjcik, R. Chulist, A. Szewczyk, J. Dutkiewicz, and W. Maziarz, *Arch. Metall. Mater.*, **68**, No. 3: 1157 (2023); https://doi.org/10.24425/amm.2023.145488
87. K. Du, Y. Zhang, G. Zhao, T. Huang, L. Liu, J. Li, X. Wang, and Z. Zhang, *Mater. Sci. Eng. A*, **890**: 145858 (2024); https://doi.org/10.1016/j.msea.2023.145858
88. A. Evirgen, J. Ma, I. Karaman, Z.P. Luo, and Y.I. Chumlyakov, *Scr. Mater.*, **67**, No. 5: 475 (2012); https://doi.org/10.1016/j.scriptamat.2012.06.006
89. M. Czerny, G. Cios, W. Maziarz, Y. Chumlyakov, and R. Chulist, *Materials*, **13**, No. 1724: 1 (2020); https://doi.org/10.3390/ma13071724
90. C. Sobrero, C. Lauhoff, D. Langenkämper, C. Somsen, G. Eggeler, Y.I. Chumlyakov, T. Niendorf, and P. Krooß, *Mater. Lett.*, **291**: 129430 (2021); https://doi.org/10.1016/j.matlet.2021.129430
91. H. Fu, H. Zhao, Y. Zhang, and J. Xie, *Procedia Eng.*, **207**: 1505 (2017); https://doi.org/10.1016/j.proeng.2017.10.1084
92. L.-W. Tseng, *J. Chinese Inst. Eng.*, **45**, No. 2: 109 (2022); https://doi.org/10.1080/02533839.2021.2012517
93. H. Fu, H. Zhao, S. Song, Z. Zhang, and J. Xie, *J. Alloys Compd.*, **686**: 1008 (2016); https://doi.org/10.1016/j.jallcom.2016.06.273
94. R. Chulist, M. Prokopowicz, W. Maziarz, P. Ostachowski, and N. Schell, *Int. J. Mater. Res.*, **110**, No. 1: 70 (2019); https://doi.org/10.3139/146.111688
95. E.C. Andrade, H.H. Bernardi, and J. Otubo, *Mater. Res.*, **17**, No. 3: 583 (2014); https://doi.org/10.1590/S1516-14392014005000072
96. G.S. Firstov, Yu.M. Koval, V.S. Filatova, V.V. Odnosum, G. Gerstein, and H.J. Maier, *Prog. Phys. Met.*, **24**, No. 4: 819 (2023); https://doi.org/10.15407/ufm.24.04.819
97. Yu.M. Koval, V.V. Odnosum, Vyach. M. Slipchenko, V.S. Filatova, A.S. Filatov, O.A. Shcheretskyi, and G.S. Firstov, *Metallofiz. Noveishie Tekhnol.*, **46**, No. 9: 933 (2024); https://doi.org/10.15407/mfint.46.09.0933
98. W. Zheng, P. Tan, J. Li, H. Wang, Y. Liu, and Z. Xian, *Struct. Control Heal. Monit.*, **2023**: 1 (2023); https://doi.org/10.1155/2023/5497731

Received 03.09.2024
Final version 28.01.2025

М.Ю. Хасбі[1,2], *Ефенді*[2], *Н. Соф'ян*[1,3]
[1] Кафедра металургії та матеріалознавства,
інженерний факультет,
Університет Індонезія, 16424 Депок, Індонезія
[2] Науково-дослідний центр металургії,
Національна аґенція досліджень та інновацій Індонезії,
Танґеранґ Селатан, 15314 Бантен, Індонезія
[3] Центр перспективних досліджень матеріалів,
інженерний факультет,
Університет Індонезія, 16424 Депок, Індонезія

СИСТЕМАТИЧНИЙ ОГЛЯД НАДПРУЖНІХ СПЛАВІВ FeNiCoAlTaB

Сплави з пам'яттю форми (ПФ) на основі заліза привернули значну увагу завдяки своїм унікальним властивостям і потенційним застосуванням. Серед них полікристалічний сплав Fe–Ni–Co–Al–Ta–B виділяється як перспективна альтернатива сплавам із ПФ на основі NiTi через свою чудову надпружну поведінку. Надпружні властивості сплавів із ПФ на основі заліза нерозривно пов'язані з термопружною природою їхньої мартенситної структури. Така структура досягається в результаті поєднання відповідних процесів виготовлення та термомеханічного оброблення. Ці процеси сприяють утворенню преципітатів і розвитку домінувальної текстури вздовж певних напрямків і площин. У попередніх дослідженнях встановлено чудову здатність до надпружності сплаву Fe–Ni–Co–Al–Ta–B — значення деформації становило 13,5 % за кімнатної температури. Цього вдалося досягти завдяки процесу виготовлення холодною прокаткою, який включає екстремальну деформацію в 98,6 %. Однак за цього процесу одержували надзвичайно тонкі листи (у 0,2 мм завтовшки), що створювало проблеми для практичного застосування через обмежений розмір і чинник форми. Для подальшого вдосконалення сплавів Fe–Ni–Co–Al–Ta–B важливим є комплексний огляд, що забезпечить фундаментальне розуміння проблеми і полегшить майбутні дослідницькі зусилля шляхом узагальнення наявних даних і методик. Отже, цей огляд має на меті запропонувати поглиблене обговорення зібраних дослідницьких даних, упорядкованих відповідно до методик дослідження, що розвиваються. Збираючи та аналізуючи ці дані, оглядова робота прагне висвітлити поточний прогрес, виявити прогалини і запропонувати потенційні напрями для майбутніх досліджень сплаву Fe–Ni–Co–Al–Ta–B.

Ключові слова: леґування, Fe–Ni–Co–Al–Ta–B, сплав з пам'яттю форми, надпружність, термомеханічні оброблення.